Tribology International 112 (2017) 117–128

Contents lists available at ScienceDirect

Tribology International

journal homepage: www.elsevier.com/locate/triboint

Numerical method for the adhesive normal contact analysis based on a Dugdale approximation

M. Bazrafshan[a,b,*], M.B. de Rooij[b], M. Valefi[c], D.J. Schipper[b]

[a] Material innovation institute (M2i), P.O. box 5008, 2600GA Delft, Netherlands
[b] Laboratory for Surface Technology and Tribology, Department of Engineering Technology, University of Twente, P.O. box 217, 7500AE Enschede, Netherlands
[c] Research Department, ASML Netherlands B.V., De Run 6501, 5504 DR Veldhoven, Netherlands

ARTICLE INFO

Keywords:
Adhesion
Numerical modeling
Conjugate Gradient Method
Pull-off force
Roughness

ABSTRACT

Modeling adhesion between two contacting surfaces plays a vital role in nano-tribology. However, providing analytical models, although desirable, is mostly impossible, in particular for complex geometries. Therefore, much attention has to be paid to numerical modeling of this phenomenon. Based on the adhesive stress description of the Maugis-Dugdale model of adhesion, which is credible over a broad range of engineering applications, an extended Conjugate Gradient Method (CGM) has been developed for adhesive contact problems. To examine the accuracy of the proposed method, the common case of the adhesive contact of a rigid sphere on an elastic half-space is investigated. To further evaluate the accuracy of this method, the adhesive contact of a rigid sphere over a wavy elastic half-space is also studied for different combinations of the amplitude and wavelength. There is good agreement between the analytical solution and the values predicted by the proposed method in the force-approach curves. Moreover, the calculation of pull-off force at a bisinusoidal interface between two surfaces is carried out for various cases to study the effects of different influential parameters including work of adhesion, elastic modulus, radius curvature at a crest, and the wavelength ratio. A curve is fitted on the calculated pull-off force in order to express it as an analytical relation. Similar to the JKR and DMT expressions for the pull-off force of a rigid ball on an elastic half-plane, the fitted curve is not affected by the elastic modulus and is linearly dependent on the radius of curvature and the work of adhesion. In addition, a power law governs the relation between pull-off force and the wavelength ratio. In the end, it is shown that roughness can either increase or decrease the adhesive force at a rough interface depending on the degree of the roughness.

1. Introduction

Adhesion plays a significant role in several technological fields and serves as one of the main reliability issues while dealing with smooth surfaces in contact under relatively low normal loads such as the case of micro/nano devices [1,2]. The early research on adhesion in contact mechanics was done by Bradley who studied the adhesive contact of rigid spheres [3]. Later on, two opposing classical theories of adhesion, JKR [4], and DMT [5], for single spherical elastic contacts were presented. Although these two models take different approaches and make significantly different assumptions, they are both true. It was shown by Tabor that these two models are the two opposite extreme limits of a single theory characterized by the Tabor parameter [6]:

$$\mu = \left(\frac{R\,\Delta\gamma^2}{E^{*2} z_0^3} \right)^{1/3} \tag{1}$$

where R, $\Delta\gamma$, E^*, z_0 are the radius of the sphere, work of adhesion, the effective elastic modulus, and the equilibrium separation, ranging from 0.2 nm to 0.4 nm. The JKR model is valid for large values of the Tabor parameter, as in the case of large and compliant contacts. The DMT model, however, is suitable for low values of this parameter, as for small and stiff contacts. Following these two models, Muller *et al.* developed a numerical solution to the adhesion interaction by integrating the Lennard-Jones potential and characterized the transition from DMT to JKR by adjusting the Tabor parameter [7]. Subsequently, Maugis provided a solution to this contact problem through assuming the contribution of adhesion inside and outside the contact area, by means of a Dugdale approximation and is known as Maugis-Dugdale

* Corresponding author at: Laboratory for Surface Technology and Tribology, Department of Engineering Technology, University of Twente, P.O. box 217, 7500AE Enschede, Netherlands.

http://dx.doi.org/10.1016/j.triboint.2017.04.001
Received 22 December 2016; Received in revised form 31 March 2017; Accepted 1 April 2017
Available online 04 April 2017
0301-679X/

(MD) model [8]. He defined an adhesive parameter which is equivalent to the Tabor parameter as:

$$\lambda = \sigma_0\left(\frac{9R}{2\pi\ \Delta\gamma E^{*2}}\right)^{1/3} = 1.16\mu, \qquad \sigma_0 = \frac{16\Delta\gamma}{9\sqrt{3}\,z_0} \tag{2}$$

in which σ_0 is the maximum attractive pressure of the Lennard-Jones potential. Based on the MD model, Johnson and Greenwood constructed an adhesion map for the contact of elastic spheres [9,10].

Although the mentioned analytical models provide exact solutions to the adhesion problem, they are limited to simple and smooth geometries. Thus, researchers have resorted to numerical approaches for surfaces with a more complex geometry [11–13]. Several authors have attempted to numerically evaluate the adhesion between two rough surfaces through multi-asperity and finite element approaches. In multi-asperity models, the surface is described merely in terms of the summit geometry and the rest of the surface is discarded [14–16]. As the main limitation of this model, next to the simplified summit geometry, is the assumption of a Gaussian distribution of roughness height, which is not valid for many engineering applications, different height distributions have been implemented, all of which still have the limitation to a specific application [16–19]. Finite element models for adhesive contact problems, incorporating the Lennard-Jones potential into the framework of nonlinear continuum mechanics, have also been developed [20,21].

The roughness of a surface could be described by means of surface models, such as fractals and Fourier transforms [22–25]. In these cases, numerical simulation of an adhesive contact has been considered while taking into account the regenerated topography of the contacting surfaces and not the original topography as it is measured. Here, the measured topography of a surface can be different from the roughness details regenerated or approximated by stochastic parameters. Consequently, since the adhesion force is a function of the exact local distance between the asperities of the two contacting surfaces, changing this distance influences the corresponding local adhesive force, and thus, deviation in the adhesive behavior is expected. Therefore, the core purpose of the current study is to develop a numerical adhesive contact solver between two elastic surfaces without any assumption on or restriction to the topography of the surfaces. Restricting ourselves to this goal, the Conjugate Gradient Method (CGM) is considered. CGM is a fast and accurate numerical algorithm typically implemented for a system of linear equations and is often used in an iterative scheme [26]. Polonsky and Keer first implemented this method for non-adhesive normal contact problems [27]. Ever since, this method has been extensively exploited for various non-adhesive contact problems in order to determine the normal and tangential contact stresses and contact area [28–33].

In the present study, the CGM is extended to include a Dugdale approximation, similar to MD model of adhesion, for the adhesive stress. In this way, it is used for the adhesive contact analysis between two elastic bodies with a general complex surface geometry.

2. Adhesive parameters

Maugis represented the surface force in terms of a Dugdale cohesive zone and stated that adhesion is present up to a specific value of the separation between the two contacting bodies, named h_0. Within this separation, the attractive pressure of σ_0, is applied such that [8] (Fig. 1):

$$\Delta\gamma = \sigma_0\, h_0 \tag{3}$$

This results in $h_0 = 9\sqrt{3}\,z_0/16 = 0.974z_0$. Based on the definition of the MD model, the pressure inside the contact region is the superposition of the positive Hertzian pressure of radius a and the negative adhesive pressure. Outside the contact region, the attractive pressure is constant over a ring of inner and outer radii of a and c, in which:

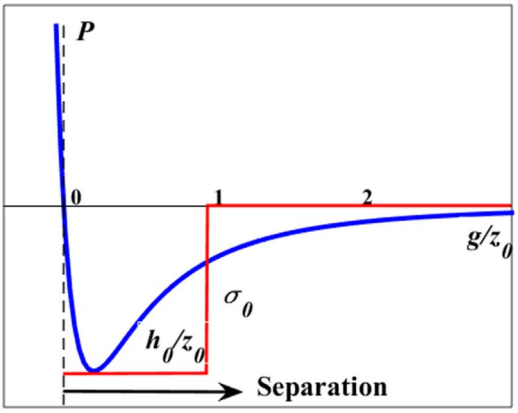

Fig. 1. Dugdale approximation (red line) of Lennard-Jones potential (blue line). (For interpretation of the references to color in this figure legend, the reader is referred to the web version of this article).

$$\varphi = \begin{cases} 0 & at \quad r = a \\ h_0 & at \quad r = c \end{cases} \tag{4}$$

where φ is the separation. The Dugdale stress, $-\sigma_0$, and the maximum separation, h_0, are the two adhesive parameters that will be used in the proposed algorithm for the adhesive normal contact between two bodies.

3. Problem definition

When two rough surfaces are brought into contact, the generated normal stress (pressure) deforms the surfaces. The composite deformation of the two surfaces, $u(x, y)$ due to the applied pressure,$P(x, y)$ over the region Ω is given by:

$$u(x, y) = \int_{\Omega} k(x - \zeta, y - \eta)P(\zeta, \eta)d\zeta d\eta \tag{5}$$

where x and y are the spatial coordinates and $k(x, y)$ is the Boussinesq kernel function and is expressed as [34]:

$$k(x, y) = \frac{1}{\pi E^*}\frac{1}{\sqrt{x^2 + y^2}}, \qquad \frac{1}{E^*} = \frac{1 - \nu_1^2}{E_1} + \frac{1 - \nu_2^2}{E_2} \tag{6}$$

in which E_i, ν_i, $i = 1, 2$ are the elastic moduli and Poisson ratios of the two contacting surfaces. If the separation between these two surfaces before and after the deformation are denoted by $h(x, y)$ and $g(x, y)$, they can be related to the deformation $u(x, y)$ as:

$$g(x, y) = u(x, y) + h(x, y) - \delta \tag{7}$$

where δ is the rigid approach of the two surfaces (Fig. 2). The non-adhesive contact problem necessitates the pressure to be positive at contacting areas, where there is no separation between the two surfaces (where $g(x, y) = 0$). On the other hand, at separate areas (where $g(x, y) > 0$), the pressure must be zero. Moreover, the pressure distribution must balance the applied normal load, F_0. In other words:

$$\begin{aligned} &P(x, y) > 0 \qquad at \qquad g(x, y) = 0 \\ &P(x, y) = 0 \qquad at \qquad g(x, y) > 0 \\ &\int_{\Omega} P(x, y)\, dx\, dy = F_0 \end{aligned} \tag{8}$$

The adhesive contact problem is, nevertheless, different from the definition by Eq. (8). For an adhesive contact problem, there is a negative stress between separated areas described by the Lennard-Jones potential as an explicit function of the local separation. As stated in the previous section, the MD model of adhesion assumes this dependence to be a step function of the local separation (by means of a Dugdale approximation of the Lennard-Jones expression). Based on this description, the negative stress due to adhesion at separated areas

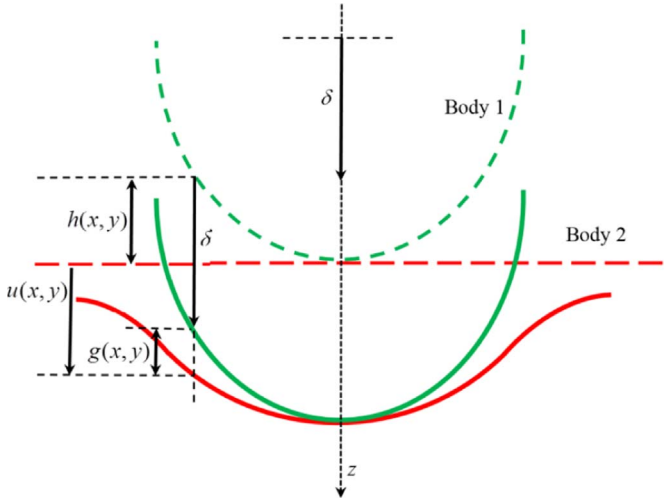

Fig. 2. The normal contact between two bodies; undeformed (dash lines) and deformed (solid lines).

is a constant value ($-\sigma_0$, the Dugdale stress which is the maximum negative stress of the Lennard-Jones potential) as long as the local separation does not exceed a specific value (named h_0 as defined in the previous section). At all other separated areas, there is no adhesive stress. It is also important to note that the pressure may take negative values at contacting areas but it is never smaller than $-\sigma_0$(therefore, the pressure transition between contacting and separate areas is continuous). This model could be mathematically summarized as:

$$\begin{aligned} &P(x, y) > -\sigma_0 \quad at \quad g(x, y) = 0 \\ &P(x, y) = -\sigma_0 \quad at \quad 0 < g(x, y) < h_0 \\ &P(x, y) = 0 \quad at \quad g(x, y) > h_0 \\ &\int_{\Omega} P(x, y)\, dx\, dy = F_0 \end{aligned} \tag{9}$$

The aim of the current study is to solve Eq. (9) for $P(x, y)$ at a general topography between two surfaces provided that the geometry of the contacting bodies ($h(x, y)$), the normal load (F_0), the mechanical properties (E and ν), and the work of adhesion ($\Delta\gamma$) are all known.

4. Numerical technique

As it was stated before, providing an analytical solution for the problem defined in previous section is only limited to simple geometries and therefore, this section aims at developing a numerical algorithm for more complex geometries.

4.1. Discretization

The first step to numerically solve Eq. (9) is to discretize the calculation area. Thus, the area Ω is divided into N^2 rectangular surface elements with grid sizes of Δx and Δy. Therefore, one can assume a piecewise constant function within each surface element for the contact pressure distribution. The discrete form of the convolution integral of Eq. (5) is then given by:

$$u_{ij} = \sum_{k=1}^{N} \sum_{l=1}^{N} K_{i-k,j-l} p_{kl}, \qquad i, j = 1, 2, \ldots, N \tag{10}$$

where u_{ij} is the surface deformation at node (i, j), p_{kl} is the uniform pressure acting upon the element centered at node (k, l), and K_{ij} are the influence coefficients, expressed as (x_i and y_j are the spatial coordinates of the node (i, j)):

$$K_{ij} = \int_{-\Delta x/2}^{\Delta x/2} \int_{-\Delta y/2}^{\Delta y/2} k(x_i - \xi, y_j - \eta)\, d\eta\, d\xi, \qquad i, j = 1, 2, \ldots, N \tag{11}$$

In practice, the DC-FFT algorithm developed by Liu et al. can be used to evaluate the linear convolution of Eq. (10), efficiently [35]. If the FFT of K_{ij} and p_{ij} are respectively denoted by $\widetilde{K}_{ij}$ and $\widetilde{p}_{ij}$, the convolution summation of Eq. (10) is performed as follows:

$$u_{ij} = IFFT\left[\widetilde{K}_{ij}.\, \widetilde{p}_{ij}\right], \qquad i, j = 1, 2, \ldots, N \tag{12}$$

where IFFT stands for Inverse Fast Fourier Transform. This method has been used by many authors [32,36,37]. One should, however, note that the FFT-based convolution leads to periodicity errors which are, due to the non-periodic nature of the contact problem, more prominent close to the boundaries of the target area. One approach to minimize this error is to expand the calculation domain by zero-padding the applied pressure outside the target area. In the present study, where needed, the calculation domain is chosen to be 2 times greater than the target domain (contact domain) [35].

4.2. CGM-based iteration scheme

Due to the fact that the only inputs to the general elastic contact problem are mechanical properties, normal force, and contacting surfaces geometry, the aim of the non-adhesive contact problem is to find the set of grid points pressure, p_{ij} which satisfies the Kuhn-Tucker complementary conditions over the target area Ω:

$$p_{ij} \geq 0, \quad g_{ij} \geq 0, \quad p_{ij} g_{ij} = 0, \qquad i, j = 1, 2, \ldots, N \tag{13}$$

Various methods have been proposed to solve this nonlinear optimization problem, among which, Conjugate Gradient Method (CGM) is regarded as one of the most prominent ones in terms of simplicity, accuracy, and convergence (readers are referred to [27] for details). To include the effect of adhesion, the definition of the mentioned problem, according to the adhesive stress description of MD model, must change as follows (the problem proposed in Section 3 is here mimicked in the discrete format):

$$\begin{aligned} &p_{ij} > -\sigma_0 \quad at \quad g_{ij} = 0 \quad (a) \\ &p_{ij} = -\sigma_0 \quad at \quad 0 < g_{ij} < h_0 \quad (b) \\ &p_{ij} = 0 \quad at \quad g_{ij} > h_0 \quad (c) \\ &\Delta x\, \Delta y \sum_{k=1}^{N} \sum_{j=1}^{N} p_{ij} = F_0 \quad (d) \end{aligned} \tag{14}$$

The following CGM algorithm is based on the one proposed by Polonsky and Keer [27]. However, in some steps, changes have been made to satisfy the conditions imposed by the presence of adhesion (described by Eq. (14)). The following procedure is an optimization algorithm to minimize the separation at contact nodes (defined as the objective function of the problem to be minimized). The whole process, as will be described, is summarized in Fig. 3 (the mathematical background of this algorithm is beyond the scope of this study and the readers are referred to [38] for details). The detailed description of this algorithm is provided next and is suitable for the readers who wish to implement it for computer programming.

Step 1. Set the initial pressure and balance the force using the approach presented in step 6. A constant pressure over the target area is a suitable initial choice.

Step 2. Initiate the iteration and calculate the deformation, u_{ij} by means of Eq. (12) and set the separation and subtract its mean value as follows:

$$\begin{aligned} &g_{ij} = u_{ij} + h_{ij} \\ &\bar{g} = \frac{1}{N_c} \sum_{(i,j) \in I_c} g_{ij} \\ &g_{ij} = g_{ij} - \bar{g} \end{aligned} \tag{15}$$

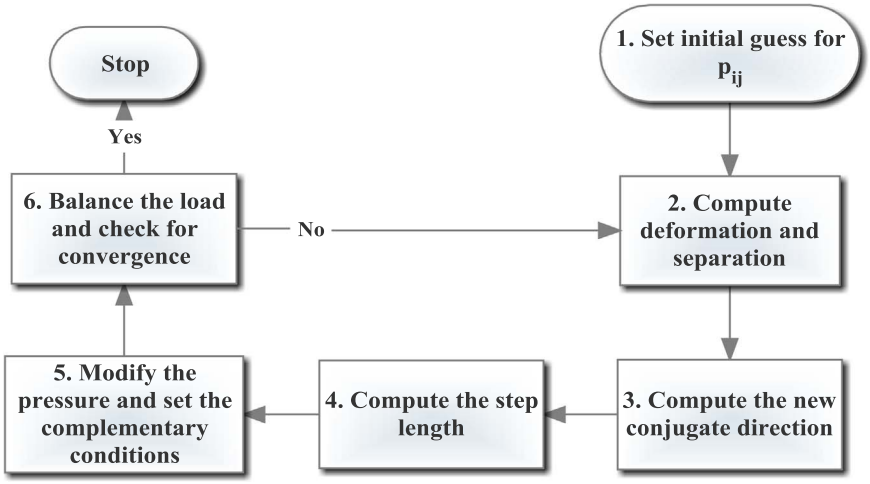

Fig. 3. Numerical algorithm, the extended CGM.

In the equation above,N_c is the number of nodes in the contact region,I_c, for which $p_{ij} > -\sigma_0$. To exclude the points with zero pressure but separation greater than h_0 from this definition for the contacting nodes, we later set the pressure at such nodes to a very high negative value such as $-1000\sigma_0$.

As stated by Polonsky and Keer, a precious feature of CG algorithm is the force balance which obviates the need for including the approach (also called penetration) between the two surfaces while computing the surface separation and therefore, enables the problem to be solved within only one level of iteration [27]. In other words, the approach is claimed to be $\bar{g}$ which is updated in each iteration.

Step 3. Compute the new conjugate direction t_{ij} as:

$$t_{ij} = \begin{cases} g_{ij} + \delta \frac{G}{G_{old}} t_{ij}, & (i,j) \in I_c \\ 0, & (i,j) \notin I_c \end{cases} \tag{16}$$

where

$$G = \sum_{(i,j) \in I_c} g_{ij}^2 \tag{17}$$

In this algorithm, the subscript "old" refers to the parameter value at the previous iteration. Therefore, G_{old} and δ are respectively set to 1 and 0 before the iteration starts.

Step 4. Store the current value of G for the next iteration by setting $G_{old} = G$. Then, do the following convolution and subtract the mean value of r_{ij} as follows:

$$\begin{aligned} r_{ij} &= \sum K_{i-k,j-l}\, t_{kl}, \\ \bar{r} &= \frac{1}{N_c} \sum_{(i,j) \in I_c} r_{ij} \\ r_{ij} &= r_{ij} - \bar{r} \end{aligned} \tag{18}$$

This convolution can be also carried out through Eq. (12). Then, calculate the step length, τ as:

$$\tau = \frac{\sum_{(i,j) \in I_c} g_{ij} t_{ij}}{\sum_{(i,j) \in I_c} r_{ij} t_{ij}} \tag{19}$$

Step 5. Store the current pressure,p_{ij} as $p_{ij_{old}}$ to be used in the next step for error estimation. At this stage, the pressure is updated by making a step in the direction t_{ij}:

$$p_{ij} = p_{ij} - \tau t_{ij}, \quad (i,j) \in I_c \tag{20}$$

Next, instead of setting all negative values of p_{ij} to zeros, as it is done for a non-adhesive elastic contact problem, set all $p_{ij} < -\sigma_0$ to $-\sigma_0$. Also, nodes with non-positive pressure and separation greater than h_0 must be set to $-1000\sigma_0$. Polonsky and Keer defined the overlap area as the set of all non-contacting nodes ($p_{ij} = 0$) at which separation is negative [27]. However, these nodes are defined here as the ones with negative pressure and separation:

$$I_{ol} = \left\{ (i,j):\ p_{ij} < 0, \quad g_{ij} < 0 \right\} \tag{21}$$

If $I_{ol} = \varnothing$, then $\delta = 1$. Otherwise, δ is set to zero and the following correction at these nodes is performed:

$$p_{ij} = p_{ij} - \tau g_{ij}, \qquad (i,j) \in I_{ol} \tag{22}$$

Since τ is always positive, the nodes in overlap area will enter the contact region by this correction.

Step 6. To balance the force, in the general elastic contact problem, the total force, F is determined by multiplying the grid area by the summation of the pressure over the whole area and then, the pressure at this stage is multiplied by the ratio F_0/F, where F_0 is the external normal load. In the present algorithm, however, we seek to keep the constant negative pressure,$-\sigma_0$ unchanged. Therefore, before applying the multiplication, the constant value of σ_0 is added to the pressure at nodes with non-zero pressure (shifted to zero) in order to keep the nodes with the constant negative pressure unaffected. Finally, the pressure is subtracted by beforehand added σ_0:

$$\begin{aligned} c_p &= \frac{F_0 + \Delta x\, \Delta y \sum_{p_{ij} > -\sigma_0} \sigma_0}{\Delta x\, \Delta y \sum_{p_{ij} > -\sigma_0} \left(p_{ij} + \sigma_0 \right)}, \\ p_{ij} &= c_p \left(p_{ij} + \sigma_0 \right) - \sigma_0, \quad \text{at nodes with} \quad p_{ij} > -\sigma_0 \end{aligned} \tag{23}$$

where Δx and Δy are the grid element sizes. It can be easily proven that Eq. (23) balances the force and the force corresponding the updated pressure distribution is the same as applied external one. Eventually, the relative error is estimated as:

$$\varepsilon = \Delta x\, \Delta y \sum \left| p_{ij_{old}} - p_{ij} \right| \tag{24}$$

If the relative error is smaller than the specified tolerance, the iteration stops. Otherwise, another iteration must be performed. It should be noted that one must set all pressures less than $-\sigma_0$ to zero before calculating the deformation in step 2 and relative error in step 6. In the end, it is very important to note that since the CGM algorithm is based on minimizing the local separation at contact points as the

residual, it is not necessary to check whether this local separation is zero when the convergence is reached.

In the present algorithm, the contribution of each element in the pressure distribution and deformation is considered separately and thus, there is no assumption in terms of the geometry. Therefore, this algorithm can be utilized at any geometry between two contacting bodies.

5. Numerical examples

In this section, to demonstrate the accuracy of the proposed method, two cases, for which the analytical solutions are available in the literature, will be numerically investigated. First, the well-known case of the adhesive contact of a rigid sphere and a flat elastic half-space will be studied. And second, the contact of a rigid sphere over a wavy half-space will be investigated. Inserting the normal force and the geometry of the contacting surfaces into the algorithm, it is expected to predict the true contact pressure and radius and then other required outputs. For the first case, the problem reduces to original MD model of adhesion for a ball-on-flat contact.

5.1. Adhesive contact of a rigid sphere over a flat elastic half-space

In this section, the ball-on-flat contact will be numerically analyzed and the results including the contact pressure, contact radius, and the imposed approach of the two bodies are compared to their analytical counterparts provided in [39]. The geometry of the sphere, as one of the inputs to the numerical algorithm, is estimated to be a parabola (as long as $r << R$) as:

$$h = \frac{r^2}{2R} \tag{25}$$

in which r is the distance from the center on the contact plane and R is the sphere radius. The other input to the numerical algorithm is the external normal force. The analytical contact radius corresponding to this force is then determined. The calculation area is extended to 2 times farther than the analytical contact radius to minimize the periodicity error to an acceptable level (as described in [35]). The whole calculating area is divided into 512×512 uniform square elements for this example. The parameter values are chosen as $E = 73$ GPa, $\nu = 0.17$, $R = 2.5mm$. Fig. 4(a) depicts the normal force vs. contact radius for various values of λ within the boundaries of JKR and DMT theories. Based on the nature of adhesion, when the normal force continuously goes down toward zero, the contact radius decreases as well, up to the point at which this force reaches zero. At this point, in contrast to the Hertzian contact model, the contact radius is non-zero. Following this trend (as shown in Fig. 4), applying a negative (pulling) force decreases the contact radius up to the complete separation of the contacting bodies. The (pulling) force required to separate the two bodies is named “pull-off” force. Further, the separation will be called jump-off since at this certain point, the molecular links between the surfaces of the bodies are abruptly broken (while the contact radius is still greater than zero). The reverse phenomenon, which is named jump-in and is literally unstable, occurs when the two bodies approach one another and at a certain separation, they jump into contact. As it is shown in Fig. 4(a), the proposed numerical approach is capable of tracking the contact behavior from a comparatively high applied force to jump-off point. However, due to its unstable nature of the contact under such conditions, this algorithm does not give a solution at the areas specified by arrows, which can be expected. This instability may also be interpreted through contact radius. It is apparent in Fig. 4(a) that for every negative force, there are two corresponding contact radii and only is the greater one stable due to its lower level of potential.

The other parameter to be evaluated is the approach. In [39], an analytical expression for this parameter as a function of contact radius was presented. Fig. 4(b) displays this relation for various values of λ. It is apparent that there is good agreement between the analytical curve and the values predicted by the numerical algorithm.

5.2. Adhesive contact of a rigid sphere over a wavy elastic half-space

In the following, the adhesive contact of a rigid sphere over a wavy elastic half-space is briefly investigated and the present numerical algorithm is employed to predict the analytical expressions provided for this problem. Fig. 5 depicts the geometry of the contact of a rigid sphere and a wavy elastic half-space. The total separation between these two surfaces is given by:

$$h(r) = \frac{r^2}{2R} + A\left(1 - \cos\frac{2\pi r}{\xi}\right) \tag{26}$$

where r, R, ξ, A are the distance from the center of contact, the radius of sphere, the wavelength and the amplitude of the wavy surface, respectively. The governing equation to find the cohesive zone m, based on MD model of adhesion, is as follows [40]:

$$\begin{aligned} 1 = {} & 2\lambda\bar{a}^2\left(\frac{\beta}{3}\right)^{2/3}\left[\sqrt{m^2-1} + (m^2-2)\tan^{-1}\sqrt{m^2-1}\right] \\ & + \frac{8}{3}\lambda^2\bar{a}\left(\frac{\beta}{3}\right)^{1/3}\left[\sqrt{m^2-1}\tan^{-1}\sqrt{m^2-1} - m + 1\right] \\ & + 2\pi\lambda\alpha\left(\frac{\beta}{3}\right)^{2/3}\left[1 - \cos 2\pi\bar{a}m - \pi^2\bar{a}H_0(2\pi\bar{a})\right. \\ & \left. + 2\pi\bar{a}H_0(2\pi\bar{a})sin^{-1}\frac{1}{m} - 2\pi\bar{a}\int_0^1 \frac{tH_0(2\pi\bar{a}t)}{\sqrt{m^2-t^2}}dt\right] \end{aligned} \tag{27}$$

The dimensionless normal force and approach are expressed as:

$$\bar{P}_m(\bar{a}) = \bar{P}_1(\bar{a}) - 4\lambda\bar{a}^2\left(\frac{\beta}{3}\right)^{2/3}\left[\sqrt{m^2-1} + m^2\tan^{-1}\sqrt{m^2-1}\right], \tag{28}$$

$$\bar{\Delta}_m = \bar{a}^2 + \bar{a}\left[\pi^2\alpha H_0(2\pi\bar{a}) - 2\lambda\left(\frac{1}{9\beta}\right)^{1/3}\sqrt{m^2-1}\right]. \tag{29}$$

where, $\bar{P}_1(\bar{a})$, the Hertzian contribution in normal force, is given by:

$$\bar{P}_1(\bar{a}) = 4\beta\left[\frac{2\bar{a}}{3} + \alpha\left(\frac{4\pi^2\bar{a}^3}{3} + \frac{\pi\bar{a}}{2}H_1(2\pi\bar{a}) - \bar{a}^2H_2(2\pi\bar{a})\right)\right] \tag{30}$$

In Eqs. (27), (29) and (30), H_i is the Struve function of order i (the Struve functions are the solutions of the non-homogeneous Bessel's differential equation) and the following dimensionless have been employed:

$$\begin{aligned} \bar{P} &= \frac{P}{\pi\,\Delta\gamma R}, \\ \beta &= \frac{\xi^3 E^*}{2\pi\,\Delta\gamma R^2}, \\ a &= \frac{a}{\xi}, \\ \bar{\Delta} &= \frac{\Delta R}{\xi^2}, \\ \alpha &= \frac{AR}{\xi^2} \end{aligned} \tag{31}$$

Eqs. (27)–(31) fully describe the MD adhesive contact problem between a rigid sphere and a wavy elastic half-space. Having in hand the external normal force, one must solve Eqs. (27) and (28) for m and $\bar{a}$, then, Eq. (29) is used to compute the normal approach (for more

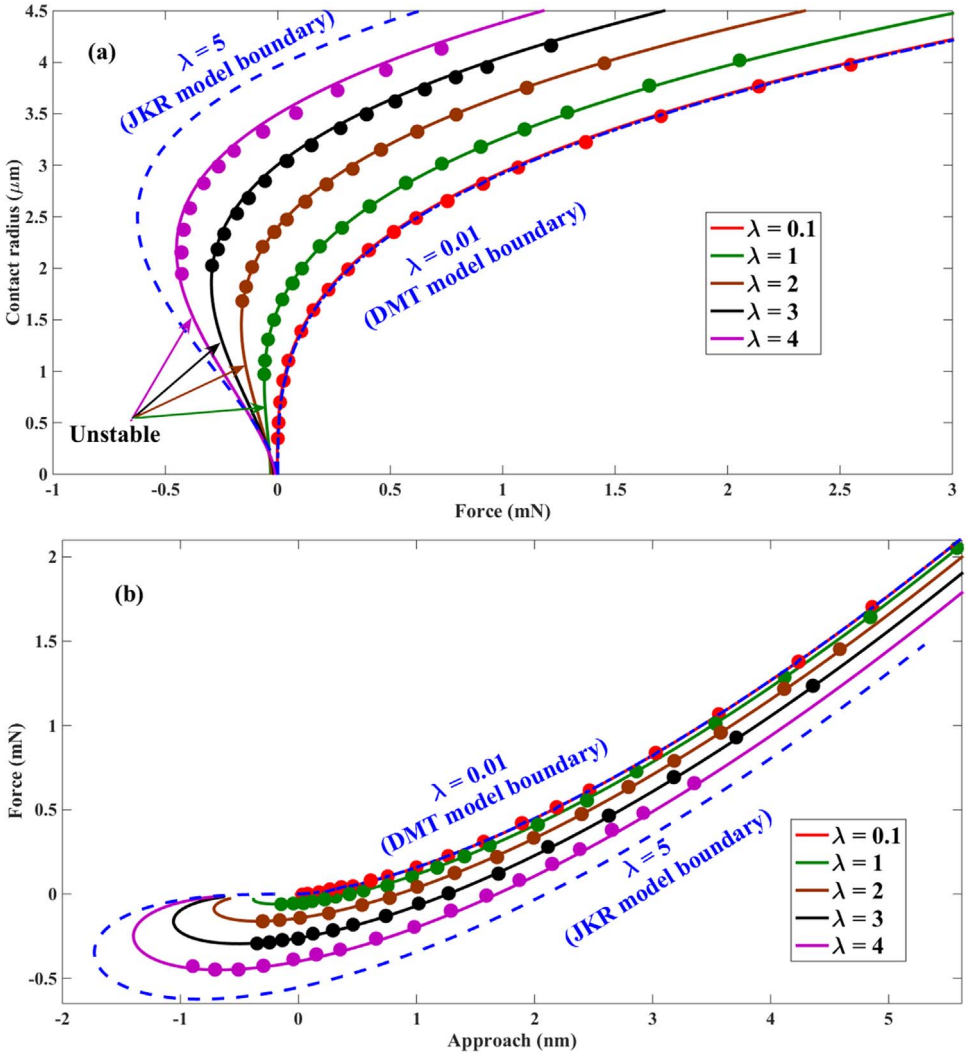

Fig. 4. (a) Variation of contact radius with normal force, (b) Variation of normal force with approach, for different values of λ. Solid lines and dots are respectively due to the MD model and (current) numerical expressions for pressure.

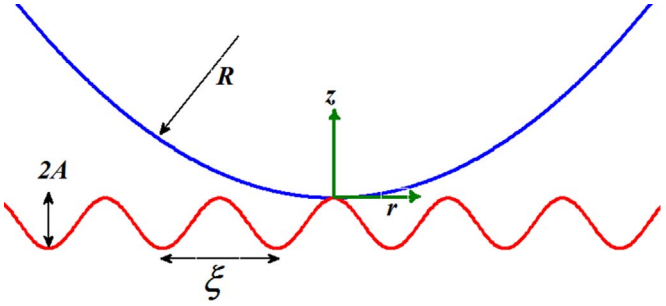

Fig. 5. Schematic representation of the contact of a rigid sphere over a wavy elastic half-space.

details refer to [40]).

To examine the accuracy of the present numerical algorithm, the external normal force and the geometrical characteristics of this type of contact are inserted into it and it is expected to predict the contact radius and approach given by the analytical expressions of Eqs. (27)–(30). The numerical values for parameters in this problem are considered the same as those of Section 5.1. The wavelength of the wavy surface is also chosen to be $0.8\mu m$. Fig. 6 shows the variation of normal force with approach for different values of λ for three different geometries of the wavy surface, specified by $\alpha = 0.1$,$\alpha = 0.2$, and $\alpha = 0.3$. As it can be seen in this figure, there is good agreement between the analytical solution and results by the numerical algorithm. Again, for every negative force, similar to the case of the ball-on-flat contact, theoretically, there are more than one corresponding approaches, only one of which is physically stable and the numerical algorithm can only capture this stable state. This behavior is observable in Fig. 6 through a number of jumps in each curve. This phenomenon, which causes energy dissipation and toughening of the contact interface, indicates that models which assume reversible approach and separation processes neglect a principal mechanism for interface toughening [40].

6. Pull-off force of a bisinusoidal interface

One of the simplest analytical representations for topography between two rough surfaces is the bisinusoidal profile which expresses a mono-modal distribution of asperities with two crossing rough waves. This combined interface could be created when one of the contacting surfaces is flat and the other one has a bisinusoidal roughness. For those tribological applications in which adhesion needs to be taken into account, providing a precise modeling is crucial. For detachment process, specifically, it is highly required to have an estimation of the pulling force needed to detach the contacting surfaces. This section aims at proposing an analytical expression for the pull-off force at a bisinusoidal interface as a function of mechanical and geometrical properties of the contacting bodies. This aim will be achieved through

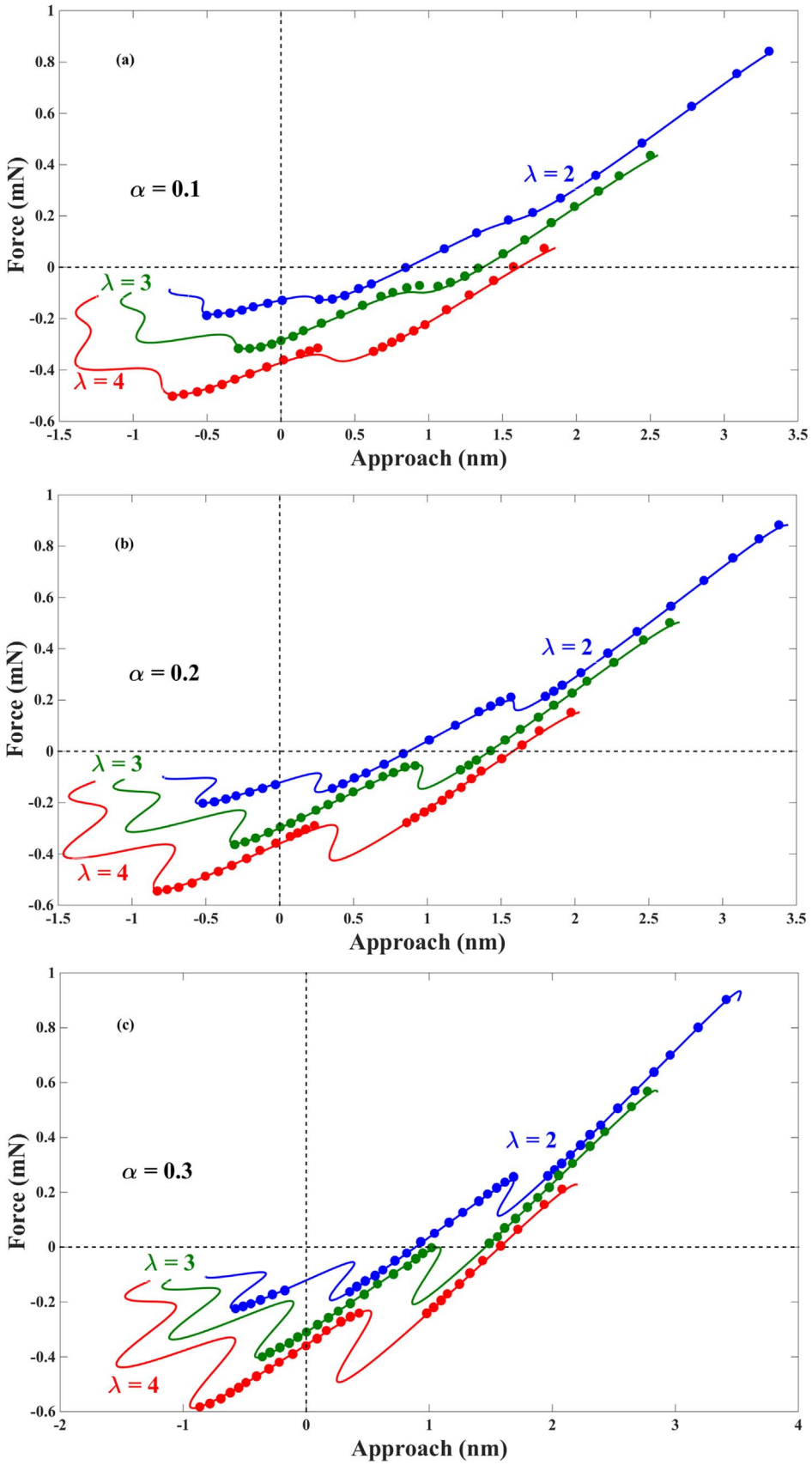

Fig. 6. Variation of normal force with approach for different values of λ in the contact of a sphere over a wavy surface, (a)$\alpha = 0.1$, (b)$\alpha = 0.2$, (c)$\alpha = 0.3$. Solid lines and dots are respectively due to the M and (current) numerical expressions for pressure.

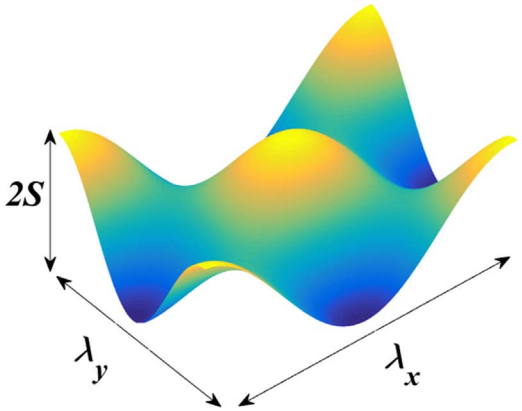

Fig. 7. A typical bisinusoidal profile.

Table 1
Parameter values for the calculation of pull-off force at a bisinusoidal interface, $S = 5nm$.

Parameter	Values
$W\ (mJ)$	30, 40, 50, 60, 70
$R\ (\mu m)$	100, 200, 300, 400, 500
E^* (GPa)	80, 90, 100, 110, 120
k	0.1, 0.3, 0.5, 0.7, 0.9

Table 2
Identified values for the unknown constants of Eq. (36) through Genetic Algorithm optimization algorithm.

Parameter	β	a	b
value	0.0	10.390	0.041

fitting a curve on the calculated pull-off forces by means of the developed numerical algorithm.

6.1. Geometry of a bisinusoidal interface

A typical bisinusoidal profile, with wavelengths λ_x and λ_y in x and y directions and amplitude S, is depicted in Fig. 7. It is worth noting that while adhering to the counter surface, the area in contact will be an ellipse whose dimensions are related to the wavelengths λ_x and λ_y(See [41] for more details).

The height of this profile is described as:

$$h(x, y) = S\cos\left(\frac{2\pi x}{\lambda_x}\right)\cos\left(\frac{2\pi y}{\lambda_y}\right), \quad -\frac{\lambda_x}{2} < x < \frac{\lambda_x}{2}, \quad -\frac{\lambda_y}{2} < y < \frac{\lambda_y}{2} \tag{32}$$

It must be noted that since this profile is originally periodic, there is no need to expand the computation domain before using DFT. The effective radius of curvature of this profile is also expressed as:

$$R_c = \sqrt{R_x R_y} \tag{33}$$

where R_x and R_y are the radii of curvature in x and y directions, respectively and are obtained through the second derivative of the surface profile as [34]:

$$R_x = \frac{\lambda_x^2}{4\pi^2 S}, \quad R_y = \frac{\lambda_y^2}{4\pi^2 S} \tag{34}$$

The wavelength ratio is also defined as:

$$k = \frac{\lambda_y}{\lambda_x}, \quad \lambda_y \le \lambda_x \tag{35}$$

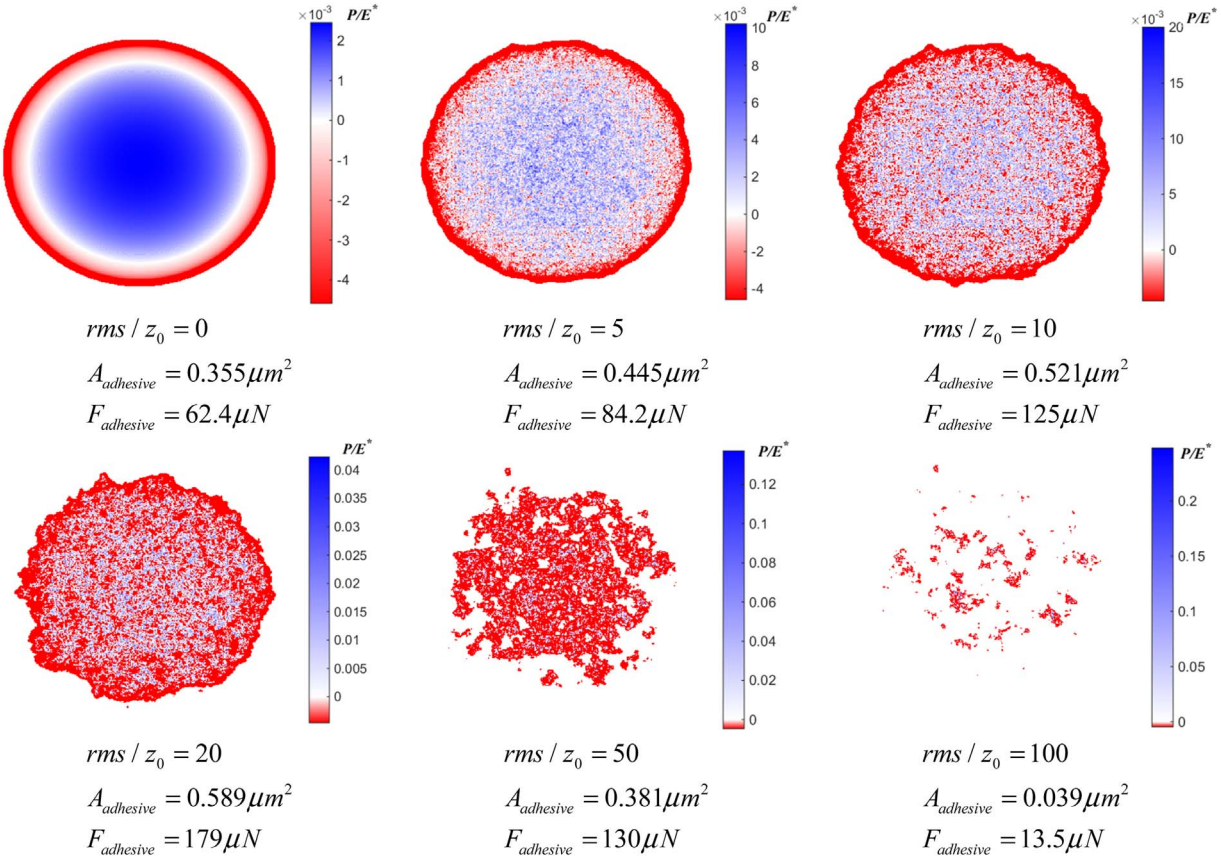

Fig. 8. Contact pressure for a smooth and rough ball of different roughness rms on a smooth flat at the same normal load for $\mu = 2$.

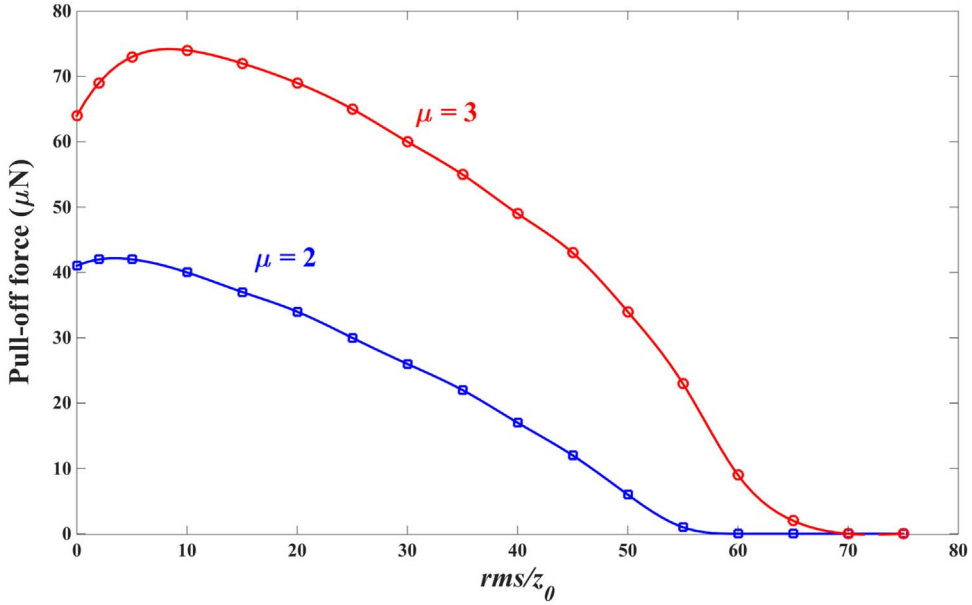

Fig. 9. The variation of pull-off force vs the roughness rms.

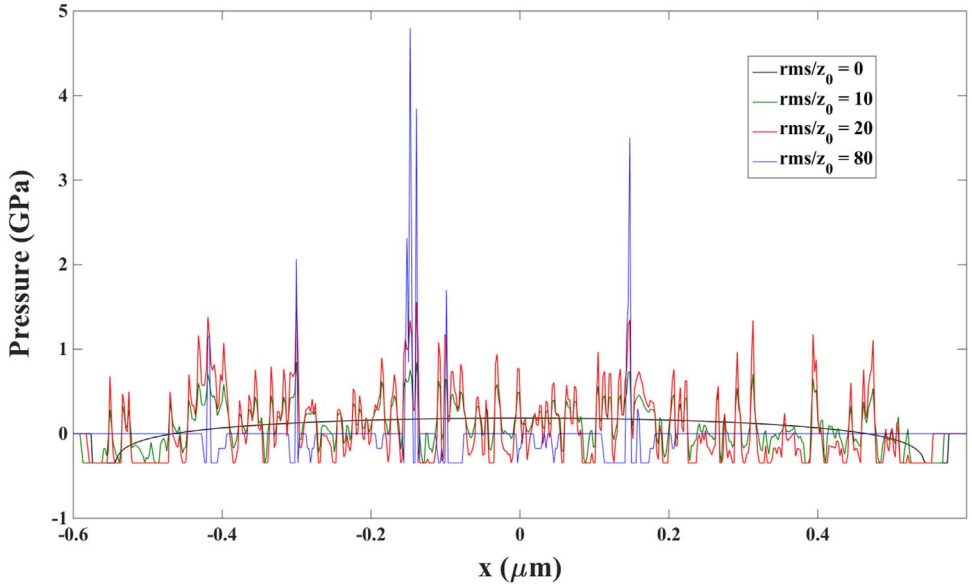

Fig. 10. The effect of roughness rms on the contact pressure for $\mu = 2$.

6.2. Analysis

The pull-off condition that is dealt with in this section assumes the contact to be only at the crests. To include any possible effect of the mechanical and geometrical parameters on the pull-off force, various values are chosen for the work of adhesion, elastic modulus, radius of curvature at a crest, and the wavelength ratio. These values are presented in Table 1. It is very important to note that S, R_c, and k fully define a unique bisinusoidal interface geometry. Each of the parameters in Table 1 takes 5 different values. Therefore, there are $5^4 = 625$ different combinations of these parameters. One should, of course, note that the Tabor parameter for any of these combinations is within the MD boundaries. By means of the proposed numerical algorithm, the pull off force is calculated through generating the force-approach curve and finding the largest negative force on the curve for all these combinations.

6.3. Curve fitting on the pull-off force results

For the mentioned 625 different combinations of mechanical and geometrical parameters, presented in Table 1, the pull-off force at the bisinusoidal interface is calculated. At this stage, we aim at fitting a curve on these calculated values to express the pull-off force at such an interface as an explicit function of the mentioned parameters. The general form of the curve is chosen to be:

$$f_{pull-off} = aE^{*\beta}R_c^{1+\beta}\Delta\gamma^{1-\beta}k^b \tag{36}$$

where a, b, β are unknown constants to be identified. The powers of E^*, R_c, $\Delta\gamma$ terms are expressed as functions of β in such a way to keep the physical dimension in both sides the same, i.e. Newton. Through an optimization algorithm, one can find the optimum set of the mentioned constants which makes the general function of Eq. (36) fit best to the calculated pull-off forces. The resulting constants are presented in Table 2.

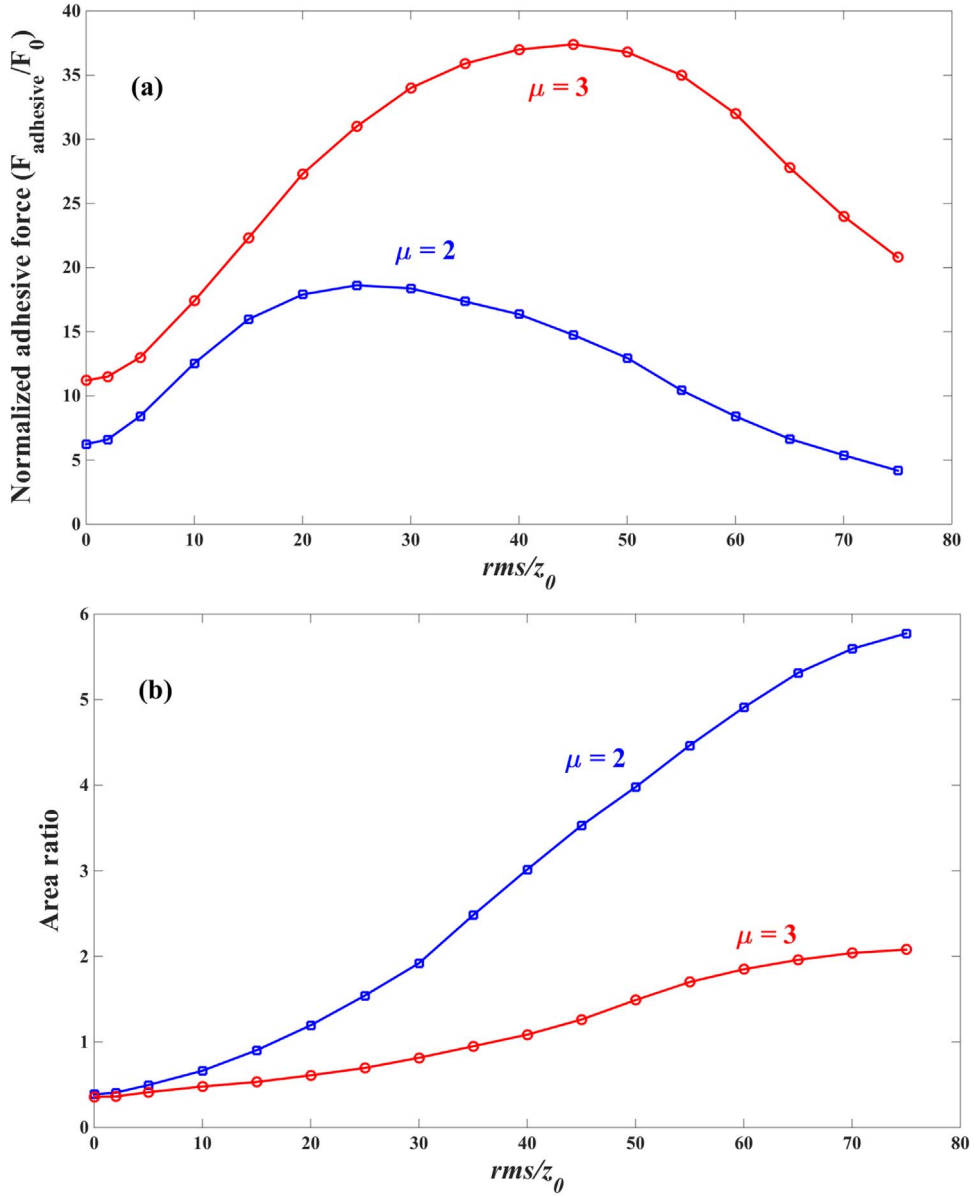

Fig. 11. The effect of roughness rms on (a) the normalized adhesive force and (b) the area ratio.

The identified values imply that the pull-off force is not dependent on the effective elastic modulus of the contacting bodies. In addition, this pull-off force is linearly dependent on both radius of curvature and work of adhesion which is identical to the JKR and DMT predictions of the pull-off force of a rigid ball over an elastic half-space. For the contact of a sphere of radius R and a half-plane, if we define $F_{pull-off} = n_{model} R\Delta\gamma$, we will have $n_{JKR} = 3\pi/2 = 4.71$, $n_{DMT} = 2\pi$ and $n_{JKR} < n_{MD} < n_{DMT}$[34]. Similarly, considering the fact that the surface investigated in this section (Fig. 7) effectively includes 2 crests (1 in the center and 4 quarters in the corners), the mentioned linearity constant for a circular area in contact when $k = 1$, caused at a single crest, is $a/2 = 5.20$. Hence, for $k = 1$ we have $n_{JKR} < n_{MD}^{Bi-sinusoidal} = 5.20 < n_{DMT}$. This consistence ascertains the validity of the fitted curve. Further, this value implies that if this relation is used to estimate the pull-off force in case of very large or small values of the Tabor parameter (corresponding to the JKR and DMT theories, respectively), the absolute value for error will be 10.4% and 16.1%, respectively.

7. The roll of roughness in the contact pressure

As stated before, the proposed algorithm does not make any assumption about how roughness is distributed over the contacting surfaces. The roughness could be either a measured roughness or a generated surface texture. The former one is applicable when the surface roughness is measured, for instance, by an Atomic Force Microscope (AFM). The latter one could be implemented to design a surface roughness and study the effects of different roughness parameters such as rms, skewness, and kurtosis. In both cases, the proposed algorithm can be used to study the adhesive behavior. In this section, we aim at studying the effect of roughness rms on the adhesive contact between a smooth ball of radius $R_b = 100\mu m$ and a rough half-space. The method proposed by Hu and Tonder has been implemented to numerically generate a Gaussian rough surface [42]. The rough profile is first subtracted by its arithmetic average value and then scaled in the vertical direction to create rough surfaces with different values of rms and keep the spatial distribution of peaks and valleys the same [12]. The mentioned subtraction is necessary in order

to keep higher order statistical parameters such as skewness and kurtosis unaffected. This technique enables one to isolate the effect of varying roughness rms and maintain the same distribution of asperities, since different distributions of asperities (even with same rms) lead to different adhesive behaviors.

Fig. 8 depicts the normalized contact pressure at this contact for different values of the roughness rms at the same normal load and for Tabor parameter $\mu = 2$. It is well-known that the roughness can reduce the adhesive force. However, it is apparent that the small amount of roughness rms can cause a large zone within the macro contact (and especially close to the contact boundary) to experience a small separation (smaller than h_0), where the adhesive stress is maximum. As we further increase the roughness rms, the majority of the contact zone is separated by greater distances (greater than h_0), and experiences no adhesive forces. Only local areas surrounding the asperities with a positive pressure are in the zone for a high adhesive force. This trend can be realized through the adhesive area and force ($A_{adhesive}$ and $F_{adhesive}$) in Fig. 8. A similar behavior is observed in Fig. 9 which shows the variation of pull-off force for this configuration versus roughness rms for two different values of Tabor parameter. It can be seen that the pull-off force first increases with the roughness rms and then decreases.

Fig. 10 depicts the effect of roughness rms on the contact pressure distribution at $F_0 = 10\mu N$. As the rms increases, the positive contact pressure scales up since the asperities locations remain the same (unless the increase in the roughness rms makes the asperity separate from the counter surface and experience a negative or zero stress depending on the local separation). However, at nodes with a negative pressure, the pressure scales down to $-\sigma_0$ and then disappears as soon as the local separation exceeds h_0.

The effect of roughness rms on the adhesive force normalized by the total normal force ($F_0 = 10\mu N$) is shown in Fig. 11(a) for two different values of the Tabor parameter. Increasing the roughness rms, as discussed for Fig. 8, first increases and then decreases. Fig. 11(b) depicts the effect of roughness rms on the area ratio, defined as the ratio of integral of the area with a negative stress to the contact area. As the roughness increases, the adhesive area decreases; yet, the decrease in the contact area is greater which, in total, leads to an increase in this ratio. It is worth noting that at all rms values, a higher Tabor parameter predicts a lower area ratio since a higher Tabor parameter corresponds to a higher work of adhesion and thus a higher contact area, which leads to a lower area ratio.

8. Conclusion

In this paper, the Conjugate Gradient Method (CGM) was extended for adhesive contact analyses between two elastic bodies with a general geometry (either rough or smooth of any shape) based on the assumptions of the Maugis-Dugdale model of adhesion. The accuracy of the proposed algorithm was examined through the conventional case of ball-on-flat adhesive contact and later, the contact of a ball over a wavy surface. Then, by means of the proposed algorithm, the pull-off force at a bisinusoidal interface was calculated for various cases of different geometrical and mechanical properties and a curve as a function of all these parameters was fitted on the calculated pull-off forces. The fitted curve showed no dependence on the elastic modulus, but a linear trend vs. radius of curvature and work of adhesion. In the end, the contact between a smooth flat and a rough ball was considered. It was shown that small degrees of roughness can increase the pull-off force, adhesive force, and area ratio.

Acknowledgment

The authors would like to express their gratitude to ASML Company, Veldhoven, the Netherlands (www.asml.com) for the financial support of this research project. This research was carried out under project number S61.7.13492 in the framework of the Partnership Program of the Materials Innovation Institute M2i (www.m2i.nl) and the Technology Foundation STW (www.stw.nl), which is a part of the Netherlands Organization for Scientific Research (www.nwo.nl).

References

[1] Stamatakis K, Tien C. A simple model of cross-flow filtration based on particle adhesion. AIChE J 1993;39:1292–302.
[2] Horton JC, German CS, Allen S, Davies MC, Roberts CJ, Tendler SJ, et al. Characterization of particle-interactions by atomic force microscopy: effect of contact area. Pharmacol Res 2003;20:508–14.
[3] Bradley RS. The cohesive force between solid surfaces and the surface energy of solids. Philos Mag J Sci 1932;86:853–62.
[4] Johnson KL, Kendall K, Roberts AD. Surface energy and the contact of elastic solids. Proc R Soc Lond A Math Phys Sci 1971;324:301–13.
[5] Derjaguin BV, Muller VM, Toporov YP. Effect of contact deformations on the adhesion of particles. J Colloid Interface Sci 1975;53:314–26.
[6] Tabor D. Surface forces and surface interactions. J Colloid Interface Sci 1977;58:2–13.
[7] Muller VM, Derjaguin BV, Toporov YP. On two methods of calculation of the force of sticking of an elastic sphere to a rigid plane. J colloids. Interface Sci 1983;7:251–9.
[8] Maugis D. Adhesion of spheres: the JKR-DMT transition using a dugdale model. J Colloid Interface Sci 1992;150:243–69. http://dx.doi.org/10.1016/0021-9797(92)90285-T.
[9] Johnson KL, Greenwood JA. An adhesion map for the contact of elastic spheres. J Colloid Interface Sci 1997;192:326–33. http://dx.doi.org/10.1006/jcis.1997.4984.
[10] Johnson KL. Mechanics of adhesion. Tribol Int 1998;31:413. http://dx.doi.org/10.1016/S0301-679X(98)00060-7.
[11] Carbone G, Mangialardi L. Adhesion and friction of an elastic half-space in contact with a slightly wavy rigid surface. J Mech Phys Solids 2004;52:1267–87.
[12] Medina S, Dini D. A numerical model for the deterministic analysis of adhesive rough contacts down to the nano-scale. Int J Solids Struct 2014;51:2620. http://dx.doi.org/10.1016/j.ijsolstr.2014.03.033.
[13] Persson BNJ. Contact mechanics for layered materials with randomly rough surfaces. Surf Sci Rep 2006;61:201–27. http://dx.doi.org/10.1016/j.surfrep.2006.04.001.
[14] Archard JF. Elastic deformation and the laws of friction. Proc R Soc Lond Ser A Math Phys Sci 1957;243. http://dx.doi.org/10.1098/rspa.1983.0054.
[15] Greenwood JA, Williamson JPB. Contact of nominally flat surfaces. Proc R Soc Lond Ser A, Math Phys Publ 1966;295:300–19.
[16] Götzinger M, Peukert W. Particle adhesion force distributions on rough surfaces. Langmuir 2004;20:5298–303. http://dx.doi.org/10.1021/la049914f.
[17] Yu N, Polycarpou AA. Combining and contacting of two rough surfaces with asymmetric distribution of asperity heights. J Tribol 2004;126:225. http://dx.doi.org/10.1115/1.1614822.
[18] Kotwal CA, Bhushan B. Contact analysis of non-gaussian surfaces for minimum static and kinetic friction and wear. Tribol Trans 1996;39:890. http://dx.doi.org/10.1080/10402009608983609.
[19] Ardito R, Frangi A, Rizzini F, Corigliano A. Evaluation of adhesion in microsystems using equivalent rough surfaces modeled with spherical caps. Eur J Mech A/Solids 2016;57:121–31. http://dx.doi.org/10.1016/j.euromechsol.2015.12.004.
[20] Cho SS, Park S. Finite element modeling of adhesive contact using molecular potential. Tribol Int 2004;37:763. http://dx.doi.org/10.1016/j.triboint.2004.04.007.
[21] Sauer RA. A computational model for nanoscale adhesion between deformable solids and its application to Gecko Adhesion. J Adhes Sci Technol 2010;24:1807. http://dx.doi.org/10.1163/016942410X507588.
[22] Mulakaluri N, Persson BNJ. Adhesion between elastic solids with randomly rough surfaces: comparison of analytical theory with molecular-dynamics simulations. Europhys Lett 2011;96:66003. http://dx.doi.org/10.1209/0295-5075/96/66003.
[23] Carbone G, Pierro E. The influence of the fractal dimension of rough surfaces on the adhesion of elastic materials. J Adhes Sci Technol 2012;26:2555. http://dx.doi.org/10.1163/156856111X623140.
[24] Yang C, Persson BNJ, Israelachvili JN, Rosenberg K. Contact mechanics with adhesion: interfacial separation and contact area. Europhys Lett 2008;84:5. http://dx.doi.org/10.1209/0295-5075/84/46004.
[25] Muser MH. Single-asperity contact mechanics with positive and negative work of adhesion: influence of finite-range interactions and a continuum description for the squeeze-out of wetting fluids. Beilstein J Nanotechnol 2014;5:419–37. http://dx.doi.org/10.3762/bjnano.5.50.
[26] Hestenes MR, Stiefel E. Methods of conjugate gradients for solving linear systems. J Res Natl Bur Stand 1934;1952(49):409–36.
[27] Polonsky IA, Keer LM. A numerical method for solving rough contact problems based on the multi-level multi-summation and conjugate gradient techniques. Wear 1999;231:206–19. http://dx.doi.org/10.1016/S0043-1648(99)00113-1.
[28] He L, Ovaert TC. Three-dimensional rough surface contact model for anisotropic materials. J Tribol 2008;130:1–6.
[29] Nelias D, Antaluca E, Boucly V, Cretu S. A three-dimensional semianalytical model for elastic-plastic sliding contacts. J Tribol 2007;129:761–71.
[30] Vollebregt EAH. A new solver for the elastic normal contact problem using conjugate gradients, deflation, and an FFT-based preconditioner. J Comput Phys 2014;257:331–51.

[31] jian Wang T, qin Wang L, Gu L, li Zhao X. Numerical analysis of elastic coated solids in line contact. J Cent South Univ 2015;22:2470. http://dx.doi.org/10.1007/s11771-015-2775-4.
[32] Wang ZJ, Wang WZ, Hu YZ, Wang H. A numerical elastic–plastic contact model for rough surfaces. Tribol Trans 2010;53:224–38. http://dx.doi.org/10.1080/10402000903177908.
[33] Zhou K, Chen WW, Keer LM, Ai X, Sawamiphakdi K, Glaws P, et al. Multiple 3D inhomogeneous inclusions in a half space under contact loading. Mech Mater 2011;43:444–57. http://dx.doi.org/10.1016/j.mechmat.2011.02.001.
[34] Johnson KL. Contact mechanics. Cambridge: Cambridge University Press; 1985.
[35] Liu S, Wang Q, Liu G. A versatile method of discrete convolution and FFT (DC-FFT) for contact analyses. Wear 2000;243:101–11. http://dx.doi.org/10.1016/S0043-1648(00)00427-0.
[36] Elsharkawy AA, Hamrock BJ. A numerical solution for dry sliding line contact of multilayered elastic bodies. J Tribol 1993;115:237–45.
[37] Stanley HM, Kato T. An FFT-based method for rough surface contact. J Tribol 1997;119:481–5.
[38] Shewchuk JR. An introduction to the conjugate gradient method without the agonizing pain. Science 1994;80, [10.1.1.110.418., 49:64].
[39] Shi X, Polycarpou AA. Adhesive transition from noncontacting to contacting elastic spheres: extension of the Maugis-Dugdale model. J Colloid Interface Sci 2005;281:449–557. http://dx.doi.org/10.1016/j.jcis.2004.08.069.
[40] Waters JF, Lee S, Guduru PR. Mechanics of axisymmetric wavy surface adhesion: jkr-dmt transition solution. Int J Solids Struct 2009;46:1033. http://dx.doi.org/10.1016/j.ijsolstr.2008.10.013.
[41] Xu Y, Rostami A, Jackson RL. Elastic contact between a geometrically anisotropic bisinusoidal surface and a rigid base. J Tribol 2015;137:021402. http://dx.doi.org/10.1115/1.4029537.
[42] Hu YZ, Tonder K. Simulation of 3-D random rough surface by 2-D digital filter and Fourier analysis. Int J Mach Tools Manuf 1992;32:83–90. http://dx.doi.org/10.1016/0890-6955(92)90064-N.